NANO LETTERS

Letter

pubs.acs.org/NanoLett

Shape-Controlled Deterministic Assembly of Nanowires

Yunlong Zhao,[†] Jun Yao,[†] Lin Xu,[†,§] Max N. Mankin,[†] Yinbo Zhu,[⊥] Hengan Wu,[⊥] Liqiang Mai,[§] Qingjie Zhang,[§] and Charles M. Lieber[*,†,‡]

[†]Department of Chemistry and Chemical Biology and [‡]Harvard John A. Paulson School of Engineering and Applied Sciences, Harvard University, Cambridge, Massachusetts 02138, United States

[§]State Key Laboratory of Advanced Technology for Materials Synthesis and Processing, Wuhan University of Technology, Wuhan 430070, China

[⊥]CAS Key Laboratory of Mechanical Behavior and Design of Materials, Department of Modern Mechanics, University of Science and Technology of China, Hefei, Anhui 230027, China

Supporting Information

ABSTRACT: Large-scale, deterministic assembly of nanowires and nanotubes with rationally controlled geometries could expand the potential applications of one-dimensional nanomaterials in bottom-up integrated nanodevice arrays and circuits. Control of the positions of straight nanowires and nanotubes has been achieved using several assembly methods, although simultaneous control of position and geometry has not been realized. Here, we demonstrate a new concept combining simultaneous assembly and guided shaping to achieve large-scale, high-precision shape controlled deterministic assembly of nanowires. We lithographically pattern U-shaped trenches and then shear transfer nanowires to the patterned substrate wafers, where the trenches serve to define the positions and shapes of transferred nanowires. Studies using semicircular trenches defined by electron-beam lithography yielded U-shaped nanowires with radii of curvature defined by inner surface of the trenches. Wafer-scale deterministic assembly produced U-shaped nanowires for >430 000 sites with a yield of ∼90%. In addition, mechanistic studies and simulations demonstrate that shaping results in primarily elastic deformation of the nanowires and show clearly the diameter-dependent limits achievable for accessible forces. Last, this approach was used to assemble U-shaped three-dimensional nanowire field-effect transistor bioprobe arrays containing 200 individually addressable nanodevices. By combining the strengths of wafer-scale top-down fabrication with diverse and tunable properties of one-dimensional building blocks in novel structural configurations, shape-controlled deterministic nanowire assembly is expected to enable new applications in many areas including nanobioelectronics and nanophotonics.

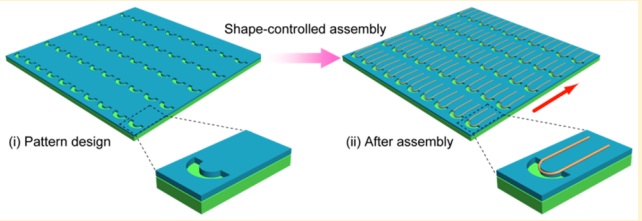

KEYWORDS: *Silicon nanowires, nanowire arrays, elastic deformation, bioelectronics, nanoelectronics, field-effect transistors*

Interest in the assembly of nanoscale wires, such as semiconductor nanowires and carbon nanotubes, has long been motivated by the development of bottom-up integrated nanodevice arrays and circuits.[1−6] Existing assembly methods[7,8] have been used to align[9−17] and in some cases deterministically position[18−22] straight nanoscale wires. These methods have used a variety of forces to achieve alignment including mechanical,[9,18,22] electric,[19,20] magnetic,[7] liquid surface tension,[10,12,15] optical,[13,17] and chemical.[14,16,21] In addition, patterning regions of selective interaction on substrates have also been used with some success for deterministic assembly.[18−22] Most recently, we have described a nanocombing assembly method[18,22] that allowed for separate anchoring and then straightening/aligning of nanowires with shear forces and showed that this could be used to assemble by deterministic design large-scale integrated finite state machine.[22]

These latter studies, which separate anchoring from alignment, suggest that the flexibility and large elastic strains sustainable in nanoscale wires[23,24] could be exploited with the combing method to assemble nanoscale wires with well-controlled curvature. Assembly of nanoscale wires with defined curvature and position could open up many opportunities not possible with straight nanoscale wires and thus represents an important target. Conceptually, to realize shape control during deterministic assembly requires that (i) applied forces are sufficiently large to bend the nanoscale wires, and (ii) the bending curvature and directions should be rationally controlled at the nanoscale. Here we address these requirements by introducing controlled curvature anchors to enable guided shaping during nanowire combing.

Our assembly method (Figure 1a) involves two key steps. First, trenches with designed shapes are patterned in a surface layer on the target substrate (Figure 1a(i)). Second, the nanowire growth substrate is flipped over and translated with a fixed normal load and specific orientation with respect to the

Received: January 22, 2016
Revised: March 15, 2016
Published: March 21, 2016

DOI: 10.1021/acs.nanolett.6b00292
Nano Lett. 2016, 16, 2644−2650

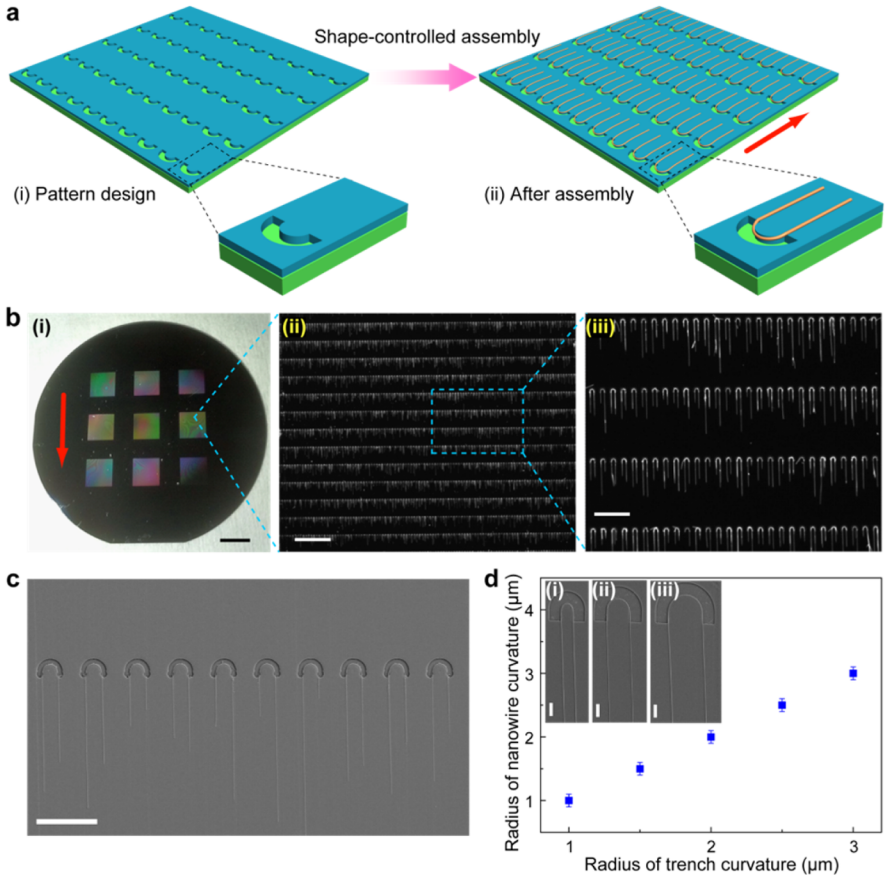

Figure 1. Shape-controlled nanowire assembly. (a) Schematic of deterministic assembly of U-shaped nanowire arrays. The red arrow (right side) shows the sliding direction of the nanowire growth substrate with respect to the target substrate. (b) Photograph and optical images of wafer-scale deterministically assembled U-shaped silicon nanowire arrays by trenches. Nanowire diameter is 80 nm. The arrow in (i) shows the sliding direction of the nanowire growth substrate with respect to the target substrate. Scale bars in (i)−(iii) are 10 mm, 200 μm, and 50 μm, respectively. (c) Representative SEM image of U-shaped silicon nanowire array. Scale bar, 20 μm. (d) Plot of the radius of nanowire curvature versus the trench radius of curvature. Nanowire diameter is 80 nm. Insets: Representative SEM images of U-shaped silicon nanowires assembled by U-shaped trenches with controlled radius, R, of curvature: (i) 1 μm; (ii) 2 μm; (iii) 3 μm. Nanowire diameter is 80 nm. Scale bars, 2 μm.

trenches over the target substrate.[18] During this latter process (Figure 1a(ii)), the trench structures serve to anchor and guide the bending of nanowires during the shear transfer process with overall alignment determined by the linear translation.

A prototypical example of our concept is shape-controlled deterministic assembly of U-shaped nanowires as it captures all of the essential elements of the assembly process; that is, the U-shape structure requires assembly to define the radius of curvature, position, and alignment. We first explored the capabilities of our approach in wafer scale deterministic assembly. First, photolithography was used to define >430 000 U-shaped trenches in nine arrays on a 3 in. wafer, where the trench radius of curvature and depth were 1.5 μm and 260 nm, respectively (see Materials and Methods in Supporting Information). This patterned target substrate was mounted on a linear translation stage, coated with high viscosity mineral oil, and then the nanowire growth substrate (randomly distributed and straight silicon nanowires: lengths, 40−80 μm; mean diameter, 80 nm) was placed on the target substrate. After the pressure was set between the patterned target and nanowire growth substrates (~4.8 N cm^{-2} in this experiment), the target substrate was translated in a direction perpendicular to the tangent of the U-shape (red arrow, Figure 1b) at a constant velocity.

Optical microscopy and scanning electron microscopy (SEM) images of the assembled nanowire arrays (Figure 1b,c) show several important features. First, U-shaped nanowires are uniformly assembled on the patterned regions of the whole wafer with pitch of adjacent nanowires of 15 μm and row-to-row pitch of 100 μm. The overall assembly yield, which is estimated from statistics from several different areas, each featuring a size of 1.5 × 1.5 mm^2 and containing 1500 sites (trench depth, 260 nm), is 86−94%. Specifically, 43−51% of the trenches contain a single nanowire. Second, nanowires are precisely anchored in the U-shaped trenches. The nanowire radii of curvature in these experiments are defined by the inner edge of the trenches, and thus it is not necessary to define nanometer width trenches to match the nanowire diameters to achieve precise assembly.

We assembled nanowires in U-shaped trenches with varying width and depth to determine how these parameters affect assembly yield (Figure S1). First, the overall yield increases with trench width, with >90% for widths ≥ 2 μm. Second, we observed that when trench depth is less than the nanowire diameter, the anchoring yield is close to zero, but the yield increases to >90% for depths ≥ ~4-times the nanowire diameter. We fabricated U-shaped trenches with different radii of curvature to rationally control the radii of curvature of nanowires. SEM images of 80 nm diameter nanowires

DOI: 10.1021/acs.nanolett.6b00292
Nano Lett. 2016, 16, 2644−2650

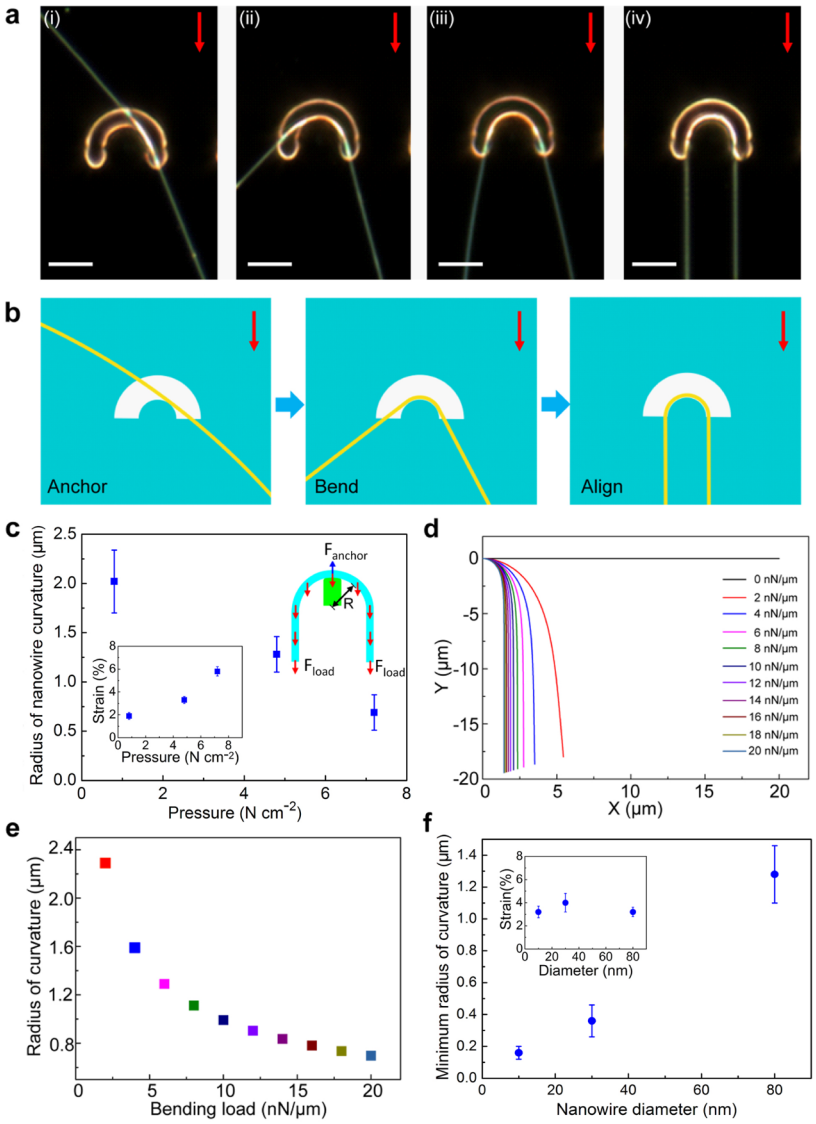

Figure 2. Shape-controlled nanowire assembly. (a) Optical images of nanowires at different stages of assembly and bending process. The red arrows show the sliding direction of the nanowire growth substrate with respect to the target substrate. Scale bars, 3 μm. (b) Schematics of anchor-bend-align assembly process. The red arrows show the sliding direction of the nanowire growth substrate with respect to the target substrate. (c) Plot of silicon nanowire R versus contact pressure. Left inset: Model and force analysis of nanowire bending during assembly. Right inset: Plot of strain of silicon nanowires versus contact pressure. Nanowire diameters are 80 nm. (d) Simulation of the deformation of the nanowire under bending loads 0−20 nN/μm. (e) The corresponding radius of curvature at the fixed end calculated from the simulation results in panel d. (f) Plot of minimum R versus nanowire diameter under standard assembly conditions (pressure = 4.8 N cm^{-2}). Inset: Plot of nanowire strain versus diameter.

assembled in trenches with radii of curvature from 1−3 μm (Figure 1d) show that the nanowire curvature closely follows the inner edge of trenches for these different radii; we address lower limits versus nanowire diameter further.

We conducted experiments and modeling to understand better the process and bending limits of shape-controlled assembly. First, we used a micromanipulator (Supporting Information) to translate the growth substrate a short about 100−200 μm distance over the target substrate trenches (vs across the entire target substrate) to yield a distribution of assembled nanowire positions from early to end stages of assembly. Representative dark field optical microscopy images (Figure 2a) reveal that the roughly straight nanowires are initially anchored on the inner edge of U-shaped trenches (Figure 2a(i)), then bend around the curved edge of the trenches (Figure 2a(ii,iii)), and finally the two arms of nanowire are aligned along the translation direction (Figure 2a(iv)). On the basis of these results and the trench width/depth dependent data (Figure S1), we suggest that shape-controlled nanowire assembly (Figure 2b) proceeds by an anchor-bend-align process. The trenches serve to initially anchor/mechanically trap nanowires, and then the shear force produced during the transfer[3,9,18,22] bends the nanowires around the shaped trench and aligns their arms to the transfer direction.

Second, we studied the effect of contact pressure on nanowire curvature by transferring 80 nm diameter nanowires into trenches with small ∼200 nm radii of curvature. SEM images (Figure S2) and analyses (Figure 2c; N = 10) for nanowires assembled with contact pressures of 0.8, 4.8, and 7.2 N cm^{-2} yield radii of 2.0 ± 0.3, 1.3 ± 0.2, and 0.7 ± 0.2 μm and estimated strains (Figure 2c, inset) of 1.9 ± 0.3, 3.3 ± 0.3, and 5.8 ± 0.4%, respectively; these values correspond to the

DOI: 10.1021/acs.nanolett.6b00292
Nano Lett. 2016, 16, 2644−2650

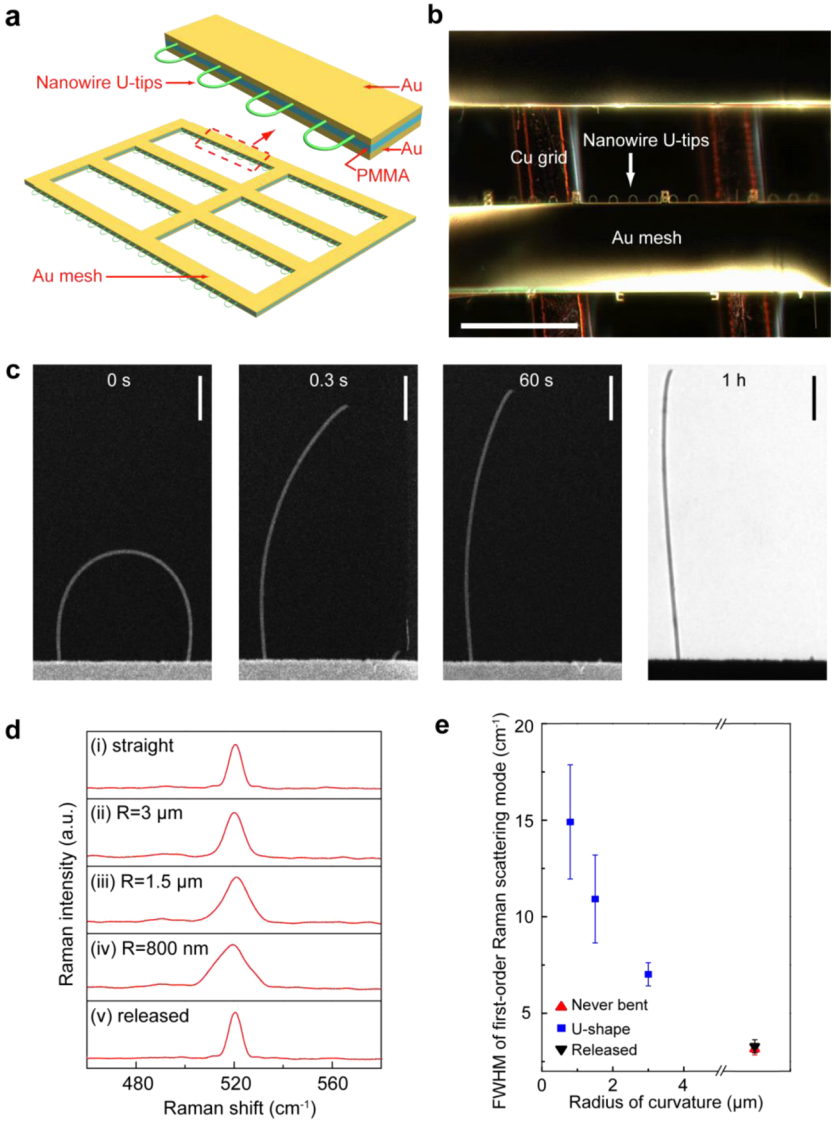

Figure 3. Strain characterization of shape-controlled nanowires. (a) Schematics highlighting the structure of the free-standing U-shaped silicon nanowire arrays with arms embedded in Au mesh. (b) Dark-field optical image of U-shaped silicon nanowire array fixed and encapsulated in a double-layer gold mesh network transferred to a copper TEM grid. Scale bar, 50 μm. (c) A time sequence of three SEM images showing the release process for a U-shaped silicon nanowire (R = 1.5 μm) after cutting by FIB. (right) TEM image of a nanowire following FIB cutting. Scale bars, 1 μm. (d) Normalized Raman spectra acquired on silicon nanowires: (i) straight/unbent nanowire; (ii–iv) U-shaped tip with R = 3.0, 1.5, and 0.8 μm, respectively; and (v) roughly straight nanowire following FIB cutting on arm remote from bend (R = 1.5 μm prior to cutting). (e) Plot of full width at half-maximum (fwhm) of the first-order Raman scattering mode versus R of assembled U-shaped silicon nanowires.

maximum strain at the surface of nanowires. A geometrically nonlinear finite element model (Supporting Information) was used to simulate the large deformation of the nanowire under uniform distributed in-plane force, F_{load}. The simulation results (Figure 2d,e) show that the radius of curvature decreases and strain increases with increasing F_{load} applied to nanowires. These results are thus consistent with the experimental data and our suggestion that increasing contact pressure during transfer yields increased F_{load}. Last, we characterized the minimum radius of curvature as a function of nanowire diameter for a fixed contact pressure of 4.8 N cm^{-2}. A summary of results for assembly of U-shaped nanowires with diameters of 10, 30, and 80 nm (Figure 2f, N = 10) yields minimum radii of curvature 0.16 ± 0.04, 0.36 ± 0.1, and 1.29 ± 0.17 μm and estimated strains of 3.2 ± 0.5, 4.0 ± 0.8, and 3.2 ± 0.4%, respectively. The 80 and 30 nm diameter nanowires were assembled on 200 nm radii of inner curvature trenches fabricated by electron-beam lithography, while the 10 nm diameter nanowires were assembled on 75 nm radii of curvature gold nanoparticles (Supporting Information; Figure S3). These results show that smaller diameter nanowires achieve smaller radii of curvature for fixed contact pressure and thus are consistent with the anchor-bend-align assembly process.

We fabricated free-standing mesh structures with assembled arrays of different radii of curvature U-shaped silicon nanowires to enable substrate-free studies of the nanowires (Supporting Information). The arms of the assembled nanowires were fixed between Au layers while the suspended U-shaped nanowire tips were left exposed (Figure 3a), and the mesh structure was transferred onto a copper transmission electron microscopy (TEM) grid (Figure 3b) for characterization. First, a focused ion beam (FIB) was used to cut one arm of suspended U-shaped nanowires (Supporting Information), and *in situ* SEM

DOI: 10.1021/acs.nanolett.6b00292
Nano Lett. 2016, 16, 2644–2650

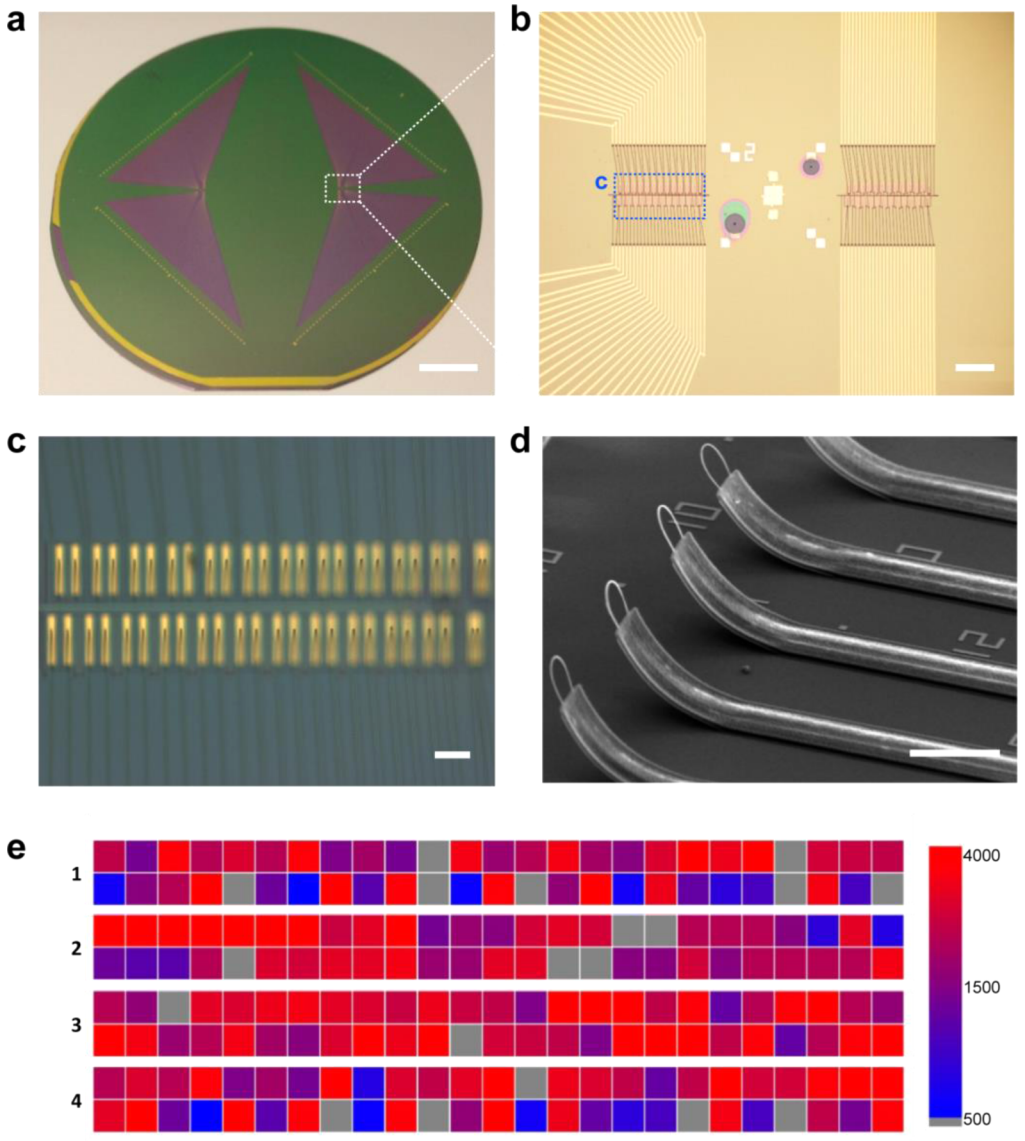

Figure 4. 3D U-shaped nanowire bioprobe arrays. (a) Photograph of a 3 in. wafer with deterministic 3D U-shaped nanowire probe arrays. Scale bar, 10 mm. (b, c) Optical microscopy images of a representative region of 3D nanowire probe arrays. Scale bars are 200 and 20 μm in panels b and c, respectively. Two-hundred total devices were fabricated in four blocks with 50 devices per block. (d) Representative tilt-view SEM image of the tips of 3D bend-up probe array. Scale bar, 10 μm. (e) Mapping of sensitivity-to-noise ratios of all 200 U-shaped silicon nanowire probes on the 3 in. wafer. 1, 2, 3, and 4 designate the four blocks. Each pixel (color from blue to red) indicates the sensitivity-to-noise (V^{-1}) of individual devices; gray pixels correspond to nonconductive devices.

imaging (Figure 3c and Supplementary Video 1) revealed that the nanowire rapidly released most of the strain within 0.3 s and then further relaxed to a nearly straight configuration after the cutting process (Figure 3c, right). These results suggest that bending is largely elastic for the assembly conditions. Second, high-resolution TEM images of suspended 80 nm diameter nanowires with 3, 1.5, and 0.8 μm radii of curvature (Figure S4) show that dislocation density in the curved portions of the nanowires increases with reduced radius of curvature. These data indicate that although strain in the nanowires is largely elastic, an inelastic component is present for these strains, which is consistent with previous nanowire studies at high strain levels.[25]

We have further investigated the nature of the strained U-shaped nanowires using Raman spectroscopy (Supporting Information). Representative spectra recorded from 80 nm diameter individual U-shaped nanowires with radii of curvature from 3−0.8 μm and straight nanowires (i.e., not bent during the assembly process and cut by FIB to relax strain) suspended from a free-standing mesh (Supporting Information) reveal several key features (Figure 3d). The first-order scattering peaks centered at ∼520 cm^{-1} are consistent with bulk Si at present in all samples. However, the full width at half-maximum (fwhm) of this mode increases from 3.1 ± 0.2 cm^{-1} in as-grown straight nanowires to 7.0 ± 0.6, 10.9 ± 2.4, and 14.9 ± 3.1 cm^{-1} as the radius of curvature decreases 3, 1.5, and 0.8 μm, respectively (N = 5; Figure 3e). Interestingly, following release by FIB-cutting, the fwhm returns to a value 3.3 ± 0.3 cm^{-1} (N = 5, Figure 3e), similar to unstrained nanowires, and is thus consistent with SEM and TEM results described earlier. Previous studies[26] indicate that the increases in fwhm can be attributed to compressive (positive frequency shift) and tensile (negative shift) strains present in bent semiconductor nanowires, which both will be present in our U-shaped nanowires.

DOI: 10.1021/acs.nanolett.6b00292
Nano Lett. 2016, 16, 2644−2650

Last, we demonstrate a potential application of shape-controlled deterministic nanowire assembly with design-based[22] fabrication of large-scale three-dimensional (3D) nanowire bioprobe arrays. We targeted U-shaped silicon nanowires in a 3D bend-up geometry since previous studies of 3D kinked nanowires highlighted the capability of these nanodevices for recording intracellular action potentials.[27] We note that overall fabrication (Supporting Information) is substantially simplified as all connections, including source/drain and interconnects, are made without the need to register to individual nanowires since all alignments can be made relative to the original U-shaped trenches used for the deterministic assembly process. A photograph (Figure 4a) and optical microscopy images (Figure 4b,c) highlight the regular structure of the probe chip with 200 individually addressable nanodevices. A representative SEM image of a portion of the probe tip region of the chip (Figure 4d) shows the regular 3D U-shaped nanowire devices with pitch of ∼20 μm.

Significantly, analysis of the device conductance values showed that 181/200 devices were conducting, giving an about 90% overall yield. Characterization of the water-gate transconductance or sensitivity and sensitivity to noise ratio for the 181 active nanodevices (Supporting Information) further yielded values for the mean ±1 standard deviation of 2.5 ± 2.0 μS/V and 2.7 ± 1.2 × 10^3 V^{-1}, respectively. A map of the sensitivity to noise values (Figure 4e) highlights the high-yield of high-sensitivity/noise devices, where 90% have values ≥ 500. These values are comparable to or better than the performance of reported individual kinked nanowire devices[28−30] and thus should be capable of improved signal recording.

In summary, we have demonstrated a new concept combining simultaneous assembly and guided shaping to achieve large-scale, high-precision shape-controlled deterministic assembly of nanowires. We lithographically pattern U-shaped trenches and then shear transfer nanowires to the patterned substrate wafers, where the trenches serve to define the positions and shapes of transferred nanowires. Studies using semicircular trenches have shown the capability for wafer-scale deterministic assembly produced U-shaped nanowires with yields of ∼90% over nearly one-half million sites. In addition, mechanistic studies and simulations have shown that the shaping process results primarily in elastic deformation of the nanowires, and they have defined diameter-dependent limits achievable for experimentally accessible forces. Last, this approach was used to assemble 3D U-shaped nanowire field-effect transistor bioprobe arrays containing 200 individually addressable nanodevices with sensitivities suitable for action potential recording from electrogenic cells.[27,28,30] In the future, we believe these 3D bioprobe arrays could be particularly attractive for probing neural networks, including measurements from acute brain slices,[31] and possibly *in vivo* recording.[32] More generally, use of shape-controlled deterministic nanowire assembly to combine the strengths of wafer-scale top-down fabrication with diverse and tunable properties of one-dimensional building blocks in novel structural configurations for new functional integrated nanodevices based on nanowire strain-engineering[33,34] and possible directions has not yet been imagined.

■ ASSOCIATED CONTENT

Supporting Information

The Supporting Information is available free of charge on the ACS Publications website at DOI: 10.1021/acs.nanolett.6b00292.

Materials and methods; dependence of nanowire anchoring yields on key trench dimensions; dependence of nanowire bending curvature on contact pressure; dependence of nanowire bending curvature on nanowire diameter; TEM images of U-shaped silicon nanowires (PDF)

SEM video recordings of the release process of a U-shaped silicon nanowire (AVI)

■ AUTHOR INFORMATION

Corresponding Author

*E-mail: cml@cmliris.harvard.edu.

Author Contributions

Y.Z. and J.Y. contributed equally to this work.

Notes

The authors declare no competing financial interest.

■ ACKNOWLEDGMENTS

C.M.L. acknowledges support from Air Force Office of Scientific Research. L.M. acknowledges support from National Basic Research Program of China (2013CB934103), International Science and Technology Corporation Program of China (2013DFA50840), and the National Natural Science Fund for Distinguished Young Scholars (51425204). M.N.M. acknowledges a Fannie and John Hertz Foundation Graduate Fellowship and a NSF Graduate Research Fellowship. This work was performed in part at the Center for Nanoscale Systems (CNS) of Harvard University.

■ REFERENCES

(1) Lu, W.; Lieber, C. M. *Nat. Mater.* **2007**, *6*, 841−850.
(2) Rutherglen, C.; Jain, D.; Burke, P. *Nat. Nanotechnol.* **2009**, *4*, 811−819.
(3) Yan, H.; Choe, H. S.; Nam, S. W.; Hu, Y.; Das, S.; Klemic, J. F.; Ellenbogen, J. C.; Lieber, C. M. *Nature* **2011**, *470*, 240−244.
(4) Takei, K.; Takahashi, T.; Ho, J. C.; Ko, H.; Gillies, A. G.; Leu, P. W.; Fearing, R. S.; Javey, A. *Nat. Mater.* **2010**, *9*, 821−826.
(5) LeMieux, M. C.; Roberts, M.; Barman, S.; Jin, Y. W.; Kim, J. M.; Bao, Z. *Science* **2008**, *321*, 101−104.
(6) Lipomi, D. J.; Vosgueritchian, M.; Tee, B. C-K.; Hellstrom, S. L.; Lee, J. A.; Fox, C. H.; Bao, Z. *Nat. Nanotechnol.* **2011**, *6*, 788−792.
(7) Wang, M. C. P.; Gates, B. D. *Mater. Today* **2009**, *12*, 34−43.
(8) Druzhinina, T.; Hoeppener, S.; Schubert, U. S. *Adv. Mater.* **2011**, *23*, 953−970.
(9) Fan, Z.; Ho, J. C.; Jacobson, Z. A.; Yerushalmi, R.; Alley, R. L.; Razavi, H.; Javey, A. *Nano Lett.* **2008**, *8*, 20−25.
(10) Tao, A.; Kim, F.; Hess, C.; Goldberger, J.; He, R.; Sun, Y.; Xia, Y.; Yang, P. *Nano Lett.* **2003**, *3*, 1229−1233.
(11) Huang, Y.; Duan, X.; Wei, Q.; Lieber, C. M. *Science* **2001**, *291*, 630−633.
(12) Yu, G.; Cao, A.; Lieber, C. M. *Nat. Nanotechnol.* **2007**, *2*, 372−377.
(13) Pauzauskie, P. J.; Radenovic, A.; Trepagnier, E.; Shroff, H.; Yang, P.; Liphardt, J. *Nat. Mater.* **2006**, *5*, 97−101.
(14) Lee, M.; Im, J.; Lee, B. Y.; Myung, S.; Kang, J.; Huang, L.; Kwon, Y.-K.; Hong, S. *Nat. Nanotechnol.* **2006**, *1*, 66−71.
(15) Cao, Q.; Han, S.; Tulevski, G. S.; Zhu, Y.; Lu, D. D.; Haensch, W. *Nat. Nanotechnol.* **2013**, *8*, 180−186.

DOI: 10.1021/acs.nanolett.6b00292
Nano Lett. 2016, 16, 2644−2650

(16) Park, H.; Afzali, A.; Han, S.-J.; Tulevski, G. S.; Franklin, A. D.; Tersoff, J.; Hannon, J. B.; Haensch, W. *Nat. Nanotechnol.* **2012**, *7*, 787−791.
(17) Agarwal, R.; Ladavac, K.; Roichman, Y.; Yu, G.; Lieber, C. M.; Grier, D. G. *Opt. Express* **2005**, *13*, 8906−8912.
(18) Yao, J.; Yan, H.; Lieber, C. M. *Nat. Nanotechnol.* **2013**, *8*, 329−335.
(19) Freer, E. M.; Grachev, O.; Duan, X.; Martin, S.; Stumbo, D. P. *Nat. Nanotechnol.* **2010**, *5*, 525−530.
(20) Li, M.; Bhiladvala, R. B.; Morrow, T. J.; Sioss, J. A.; Lew, K.-K.; Redwing, J. M.; Keating, C. D.; Mayer, T. S. *Nat. Nanotechnol.* **2008**, *3*, 88−92.
(21) Rao, S. G.; Huang, L.; Setyawan, W.; Hong, S. *Nature* **2003**, *425*, 36−37.
(22) Yao, J.; Yan, H.; Das, S.; Klemic, J. F.; Ellenbogen, J. C.; Lieber, C. M. *Proc. Natl. Acad. Sci. U. S. A.* **2014**, *111*, 2431−2435.
(23) Tang, D. M.; Ren, C.-L.; Wang, M.-S.; Wei, X.; Kawamoto, N.; Liu, C.; Bando, Y.; Mitome, M.; Fukata, N.; Golberg, D. *Nano Lett.* **2012**, *12*, 1898−1904.
(24) Superfine, R.; Falvo, M. R.; Clary, G. J.; Taylor, R. M.; Chi, V.; Brooks, F. P.; Washburn, S. *Nature* **1997**, *389*, 582−584.
(25) Wang, L.; Zheng, K.; Zhang, Z.; Han, X. *Nano Lett.* **2011**, *11*, 2382−2385.
(26) Chen, J.; Conache, G.; Pistol, M.-E.; Gray, S. M.; Borgström, M. T.; Xu, H.; Xu, H. Q.; Samuelson, L.; Håkanson, U. *Nano Lett.* **2010**, *10*, 1280−1286.
(27) Tian, B.; Cohen-Karni, T.; Qing, Q.; Duan, X.; Xie, P.; Lieber, C. M. *Science* **2010**, *329*, 830−834.
(28) Qing, Q.; Jiang, Z.; Xu, L.; Gao, R.; Mai, L.; Lieber, C. M. *Nat. Nanotechnol.* **2013**, *9*, 142−147.
(29) Xu, L.; Jiang, Z.; Qing, Q.; Mai, L.; Zhang, Q.; Lieber, C. M. *Nano Lett.* **2013**, *13*, 746−751.
(30) Xu, L.; Jiang, Z.; Mai, L.; Qing, Q. *Nano Lett.* **2014**, *14*, 3602−3607.
(31) Qing, Q.; Pal, S. K.; Tian, B.; Duan, X.; Timko, B. P.; Cohen-Karni, T.; Murthy, V. N.; Lieber, C. M. *Proc. Natl. Acad. Sci. U. S. A.* **2010**, *107*, 1882−1887.
(32) Liu, J.; Fu, T.-M.; Cheng, Z. G.; Hong, G. S.; Zhou, T.; Jin, L. H.; Duvvuri, M.; Jiang, Z.; Kruskal, P.; Xie, C.; Suo, Z. G.; Fang, Y.; Lieber, C. M. *Nat. Nanotechnol.* **2015**, *10*, 629−636.
(33) Sun, L.; Kim, D. H.; Oh, K. H.; Agarwal, R. *Nano Lett.* **2013**, *13*, 3836−3842.
(34) Cao, J.; Ertekin, E.; Srinivasan, V.; Fan, W.; Huang, S.; Zheng, H.; Yim, J. W. L.; Khanal, D. R.; Ogletree, D. F.; Grossman, J. C.; Wu, J. *Nat. Nanotechnol.* **2009**, *4*, 732−737.

DOI: 10.1021/acs.nanolett.6b00292
Nano Lett. 2016, 16, 2644−2650

Supporting Information for

Shape-Controlled Deterministic Assembly of Nanowires

Yunlong Zhao[†], Jun Yao[†], Lin Xu[†,§], Max N. Mankin[†], Yinbo Zhu[⊥], Hengan Wu[⊥], Liqiang Mai[§], Qingjie Zhang[§] & Charles M. Lieber[*,†,‡]

[†]Department of Chemistry and Chemical Biology, and [‡]Harvard John A. Paulson School of Engineering and Applied Sciences, Harvard University, Cambridge, Massachusetts 02138, United States

[§]State Key Laboratory of Advanced Technology for Materials Synthesis and Processing, Wuhan University of Technology, Wuhan 430070, China

[⊥]CAS Key Laboratory of Mechanical Behavior and Design of Materials, Department of Modern Mechanics, University of Science and Technology of China, Hefei, Anhui 230027, China

This file includes:

Materials and Methods

Nanowire synthesis. Silicon nanowires were synthesized using a gold (Au) nanoparticle-catalysed vapour-liquid-solid (VLS) process described previously.[1] Briefly, 10, 30 and 80 nm diameter Au nanoparticles (15703, 15706 and 15710, Ted Pella, Redding, CA) were dispersed on the SiO_2 surface of Si growth substrates (600 nm thermal SiO_2, Nova Electronic Materials, Flower Mound, TX). Nanowire growth was carried out at 430–455 °C. Specifically, the intrinsic nanowires were synthesized at a total pressure of 40 Torr with 2.5 standard cubic centimetres per minute (sccm) silane (SiH_4, 99.9999%, Voltaix, Branchburg, NJ) as the silicon reactant, 60 sccm hydrogen (H_2, 99.999%; Matheson, Basking Ridge, NJ) as the carrier gas. Growth temperatures of 435 °C, 450 °C, and 450 °C were used for diameters of 10, 30, and 80 nm, respectively. For the synthesis of p-type nanowires, additional 3.1 sccm diborane (B_2H_6, 100 p.p.m. in H_2, Voltaix, Branchburg, NJ) was introduced as the p-type dopant. Growth temperatures of 430 °C, 450 °C, and 450 °C were used for diameters of 10, 30, and 80 nm, respectively. Intrinsic nanowires were used for nanowire assembly and p-type nanowires were used for fabrication of bioprobe device arrays in this work. Typical growth times of 1–2 h yielded nanowires with average lengths of 40–80 μm.

Shape controlled assembly. A range of target substrates were used in our studies, including Si wafers (Nova Electronic Materials, Flower Mound, TX) with SiO_2, Si_3N_4, Au, nickel (Ni) and SU-8 polymer (SU-8 2000.5, Microchem, Inc., Westborough, MA) surface layers. The substrate surface layer was cleaned by rinsing in isopropanol (IPA, Cleanroom® MB, KMG Electronic Chemicals, Inc., Houston, TX) for 30 s followed by nitrogen drying. LOR 1A and diluted S1805 (1:2 (vol : vol) diluted in Thinner-P) (Microchem, Westborough, MA) for photolithography (PL)

or double layer polymethyl methacrylate (PMMA, 950-C2, Microchem, Westborough, MA) for electron beam lithography (EBL) was spin-coated, and PL or EBL was used to define arrays of trenches with thicknesses of ~260 nm and with shapes and widths as described in the main text. For trenches with thicknesses of ~20, ~50, ~130, and ~260 nm, diluted PMMA 950-A2 (1:1 (vol : vol) diluted in Anisole), PMMA 950-A2, PMMA 950-C2 and PMMA 950-A6 was spin-coated as resist, respectively. The minimum radii of curvature trench structures fabricated by PL and EBL were 1.5 μm and 200 nm, respectively. No additional surface modification followed exposure and development of these patterns.

Shape-controlled assembly of nanowires was carried out in a manner similar to shear-printing described elsewhere.[1-3] Briefly a target substrate patterned with an array of trenches was mounted onto a micromanipulator-controlled moveable stage, covered with mineral oil (330760, viscosity, v, $\approx$ 70 mPa•s, Sigma-Aldrich, St. Louis, MO), and then the nanowire growth substrate was brought into contact with the target substrate with controlled contact pressure (values in text). The target substrate was moved at a constant velocity of ~5 mm min^{-1} with respect to the fixed nanowire growth substrate, and then the growth substrate was removed and the target substrate rinsed with octane (98%, Sigma-Aldrich, St. Louis, MO) to remove the lubricant. The minimum radius of nanowire curvature achievable by this process was determined by using ca. 200 nm radii of curvature trenches fabricated by EBL for 80 and 30 nm diameter silicon nanowires. For 10 nm diameter silicon nanowires, 76 +/- 1.1 nm (mean +/- standard deviation) radius Au nanoparticles (15712, Ted Pella, Redding, CA; size statistics obtained from the vendor's characterization) were used as anchoring means. In this case, the Au nanoparticles were dispersed on SiO_2/Si substrate modified with poly-L-lysine (P8920, Sigma-Aldrich, St. Louis, MO), followed by deposition of ~10 nm thick Al_2O_3 film by atomic layer deposition

(ALD) at 150^{o}C (90 cycles). In addition, experiments were carried out by placing the nanowire growth substrate directly over the substrate with trenches, translating approximately 100–200 μm, and then removing the growth substrate and imaging the positions of the transferred nanowires with respect to the trenches; the data in Figure 2a was obtained in this manner.

TEM sample preparation and characterization. Arrays of U-shaped silicon nanowires with different radii of curvature were prepared for transmission electron microscopy (TEM) characterization by fixing the arms of the assembled wires between Au metal layers while leaving the suspended nanowire tips exposed for imaging. We introduced Au layers on both top and bottom of patterned PMMA for assembly as follows. (1) A Ni sacrificial layer (100 nm) was deposited on an oxidized silicon substrate by thermal evaporation (TE). (2) A square mesh gold ribbon network (100 nm) was defined on the Ni layer by EBL and TE. (3) Arrays of U-shaped 80 nm diameter silicon nanowires were patterned as described above such that the straight arms and U-tips were on top of the gold mesh and open areas, respectively. (4) PMMA under the straight arms of U-shaped nanowires was cross-linked by EBL using a dose of ~8,000 μC/cm^2. (5) A second Au mesh (100 nm thick) which was coincident in the x-y plane with the bottom mesh was defined on top of the cross-linked PMMA and deposited via TE. (6) The nickel sacrificial layer was etched in nickel etchant (TFB, Transene Company, Inc., Danvers, MA) for 1 h and then the free-standing arrays of U-shaped silicon nanowires embedded in the Au-mesh/PMMA/Au-mesh trilayer were transferred to a copper TEM grid (300 mesh Cu, Ted Pella, Redding, CA). TEM characterization (JEOL 2100, JEOL Ltd. or aberration-corrected Zeiss Libra MC TEM, Carl Zeiss AG) was carried out at a beam accelerating voltage of 200 kV. Fourier-filtered images

processed from the high-resolution TEM (HRTEM) images were used to characterize dislocations in the bent nanowires.

Strain release tests. Arrays of suspended U-shaped silicon nanowires were transferred to TEM grids as described above and introduced into a focused ion beam (FIB) instrument (dual ion/electron beam Zeiss NVision 40, Carl Zeiss AG). The FIB was used to cut one of the two suspended arms of a U-shaped nanowire (Ga^+ ions, 30 kV) while monitoring the nanowire release process *in situ* by SEM video-rate imaging (8 frames per second).

Raman spectroscopy characterization. Arrays of suspended U-shaped silicon nanowires with some nanowires cut by FIB in a free-standing mesh supported on a Cu TEM grid were placed on a glass slide. Straight nanowires that adhered in random positions on the PMMA surface (i.e., not bent during the assembly process) were also transferred and suspended in the same mesh for control measurements. Raman spectra were acquired with a LabRam Evolution Multiline Raman Spectrometer (Horiba, Kyoto, Japan) equipped with 1800 blaze/mm grating and a 100x microscope objective lens with numerical aperture (N.A.) of 0.95. A continuous-wave (CW) diode laser with a wavelength of 633 nm was used as incident light source and circularly polarized using a zero-order quarter waveplate optimized for 633 nm. The laser power was ~26 μW and the laser spot size was ~1.5 μm in diameter.

Finite element simulations of nanowire bending. A geometrically nonlinear finite element model was used to simulate the large deformations of nanowires under load. The modelling and simulations were carried out with commercial ANSYS 14.5 software. In our model, the nanowire

is considered as a linearly elastic cantilever beam with elastic modulus of 188 GPa and Poisson ratio of 0.3 characteristic of silicon.[4] The length and diameter of the cantilever beam are 20 μm and 80 nm, respectively. The in-plane forces generated during the experimental assembly process are expected to produce approximately uniform distributed bending loads, which are applied in the simulations; these uniform bending loads ranged from 0 to 20 nN/μm. The deformation of the nanowire under different loading is shown in Figure 2d. The corresponding load-dependent radii of curvature at the fixed end were calculated from the simulated results and are plotted in Figure 2e.

Bend-up nanowire probe arrays. Arrays of U-shaped silicon nanowires were used as building blocks to fabricate three-dimensional (3D) bend-up nanoprobe device arrays. Briefly, (1) a Ni sacrificial layer (100 nm) was defined by EBL and deposited on a silicon substrate (600 nm thermal SiO_2). (2) The substrate was coated with SU-8 resist (1:1 diluted SU-8R 2000.5 in cyclopentanone, Microchem, Inc., Westborough, MA), and then the bottom SU-8 support layer was defined by EBL. (3) After definition of the U-shaped PMMA trench arrays by EBL, U-shaped 10−80 nm diameter silicon nanowires were deterministically assembled in the trenches. (4) Source/drain metal contacts Cr/Pd/Cr (1.5/75/50 nm) were defined by EBL and TE. Typically, the source/drain contact separation was 1.5 μm in each probe, and the free end of the nanowire extended 2−6 μm from the source contact. (5) A top SU-8 (SU-8R 2000.5, Microchem, Inc., Westborough, MA) layer was subsequently defined by EBL to complete the passivation of the metal contacts/interconnects. (6) The nickel layer was etched (~1 h, TFB etchant, Transene Company, Inc., Danvers, MA) to yield the 3D bend-up probes. The individual nanowire probe devices were fabricated without registration to nanowires, since the patterns of bottom SU-8

passivation layer, contact electrodes and top SU-8 passivation layer, and *x*- and *y*- coordinates of U-shaped nanowires all precisely match the original trench pattern used for U-shape deterministic assembly; that is, the process follows a design-oriented fabrication approach.[5]

Device sensitivities were characterized by water-gate measurements in 1× phosphate buffered saline (PBS) with a Ag/AgCl reference electrode.[6-8] The nanowire device conductance values were measured with a DC bias of 0.5 V, and the current was converted to voltage with a current preamplifier (10^{-7} A/V, Model 1211, DL Instruments, Brooktondale, NY), and digitized at 20 kHz sampling rate (Axon Digi1440A, Molecular Devices). The sensitivity of our U-shaped silicon nanowires is 2.5 ± 2.0 μS/V. The sensitivity of our previous reported kinked silicon nanowires[6] is 8.5 ± 4.3 μS/V.

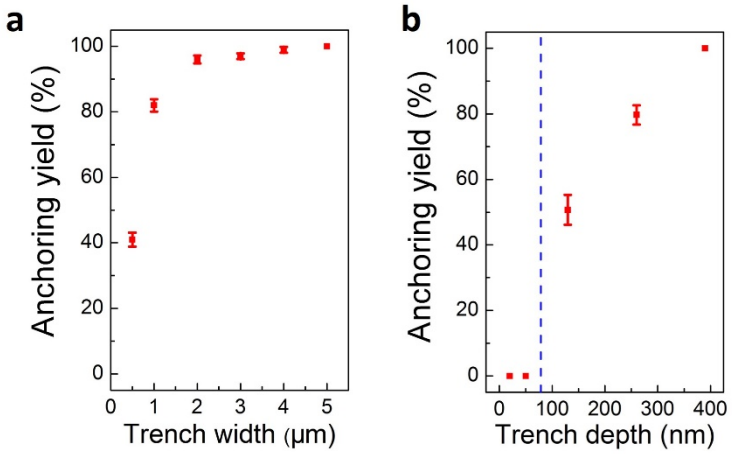

Figure S1. Dependence of nanowire anchoring yields on key trench dimensions. The nanowire anchoring yield versus trench (a) width and (b) depth. For (a), trench widths are 0.5, 1, 2, 3, 4, 5 μm and depth is fixed at 260 nm. For each data point, statistics is based on analysis of 210 sites randomly selected. For (b), trench depths are 20, 50, 130, 260, 390 nm and width is fixed at 3 μm. For each data point, statistics is based on analysis of 600 sites randomly selected. The blue vertical dashed line corresponds to the 80 nm diameter nanowires used in the measurements. These results indicate that trench width and depth can be used to optimize the anchoring yield of nanowires during assembly.

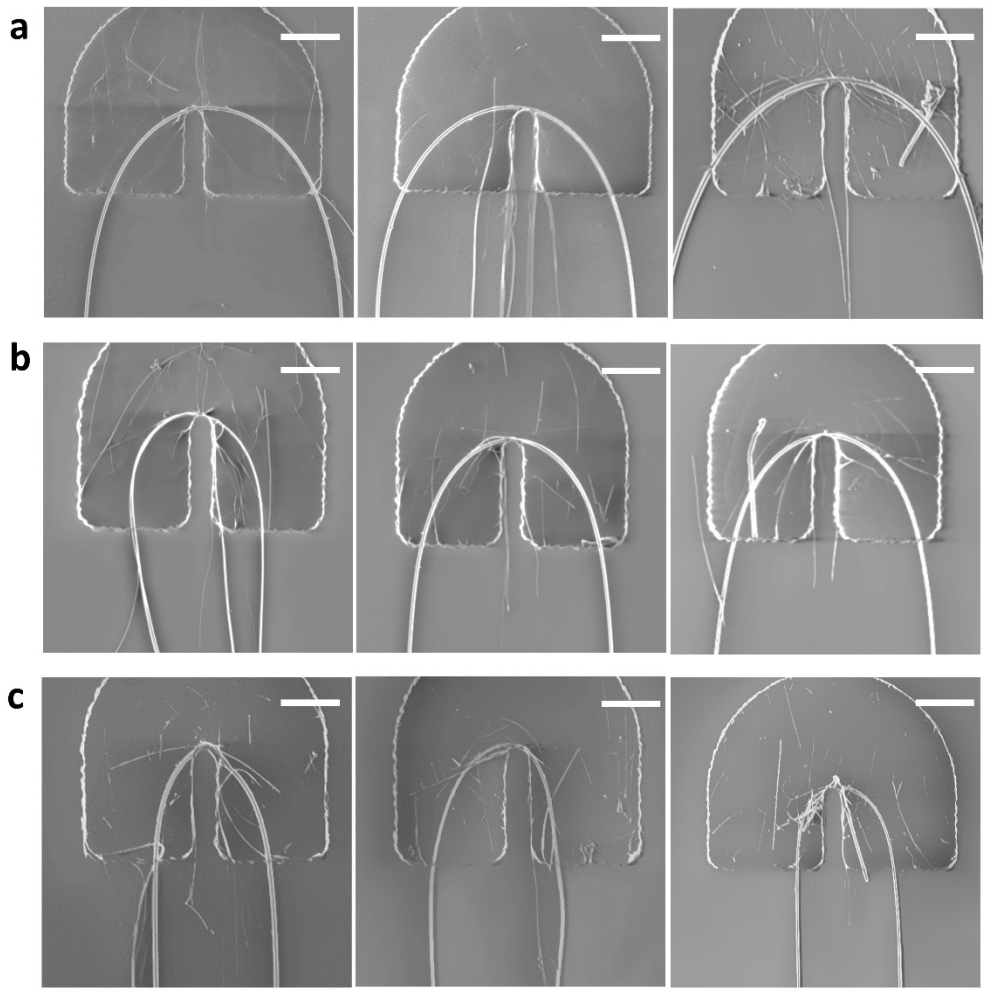

Figure S2. Dependence of nanowire bending curvature on contact pressure. Representative SEM images of 80 nm diameter silicon nanowires assembled with normal pressures of (**a**) 0.8, (**b**) 4.8 and (**c**) 7.2 N cm^{-2}. Scale bars all 1 μm. These results are consistent with increasing in-plane bending loads as the contact pressure is increased; that is, we find decreases in nanowire radius of curvature with increasing bending loads (simulation) or transfer normal pressures (experiments).

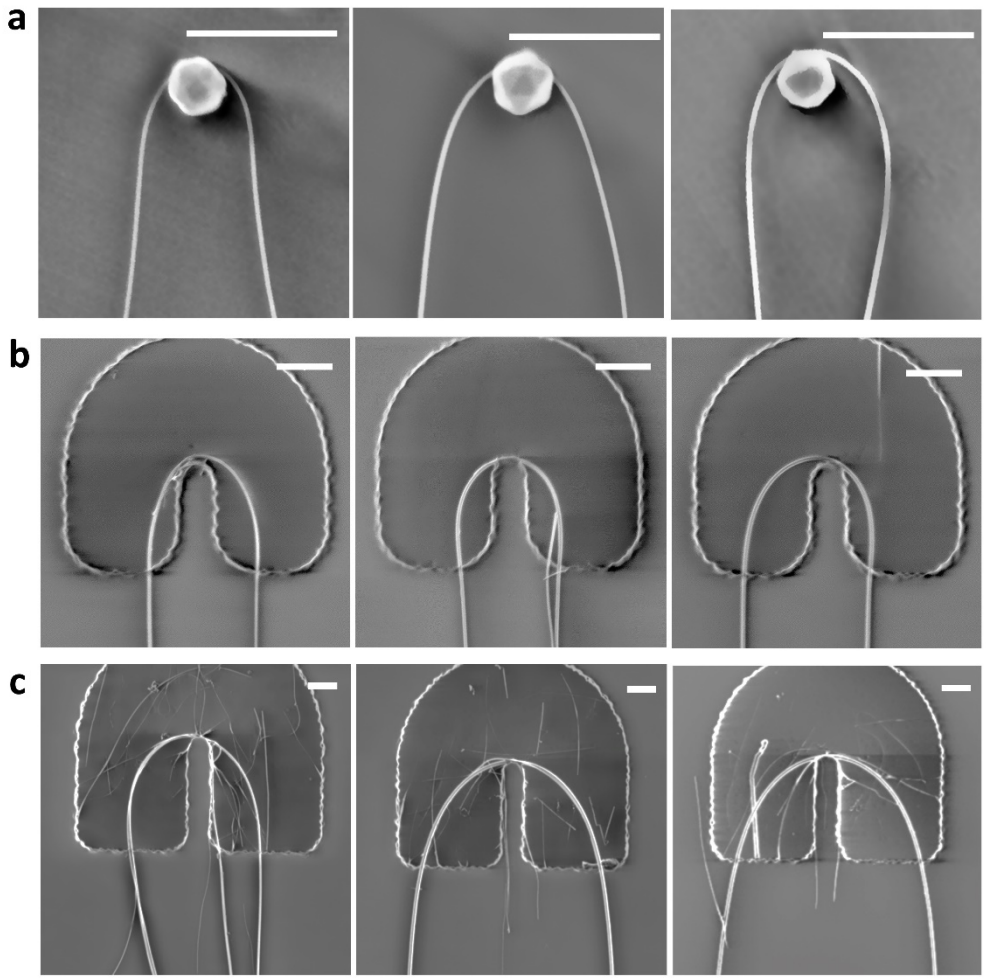

Figure S3. Dependence of nanowire bending curvature on nanowire diameter. Representative SEM images of silicon nanowires with different diameters assembled with normal pressures of 4.8 N cm^{-2}. **a**, 10 nm diameter nanowires anchored on Au particles (radii ~75 nm). **b**, 30 nm diameter nanowire anchored on trenches with depth of 130 nm, width of 1μm, and radii of inner curvature of 200 nm. **c**, 80 nm diameter nanowire anchored on trenches with depth of 260 nm, width of 3 μm, and radii of inner curvature of 200 nm. Scale bars, 500 nm.

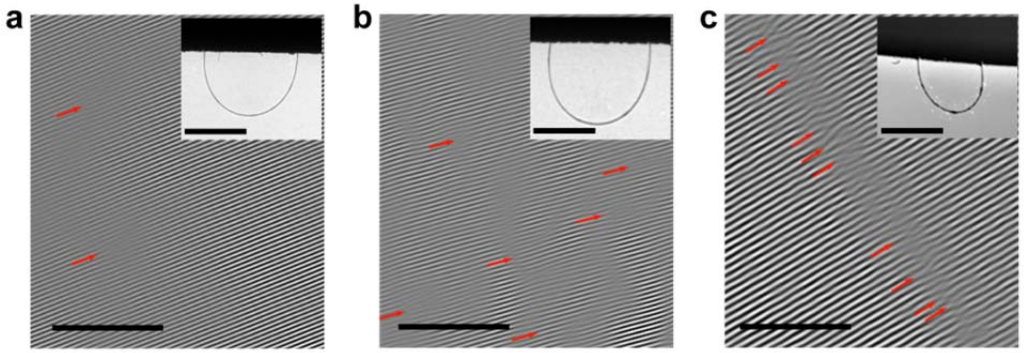

Figure S4. TEM images of U-shaped silicon nanowires. a-c, Fourier-filtered high resolution TEM images of the tips of assembled U-shaped nanowires (all nanowire diameters are 80 nm) with radii of curvature of 3.0, 1.5, and 0.8 μm in **a**, **b** and **c**, respectively. Red arrows indicate dislocations. Scale bars, 5 nm. Insets, low magnification TEM images of the U-shaped, suspended nanowires. Inset scale bars are 4, 2 and 2 μm in **a**, **b** and **c**, respectively. TEM analysis indicates that the overall dislocation density in the curved portions of the nanowires increases as the radius of curvature decreases.

Supplementary Video 1. SEM video recordings of the release process of a U-shaped silicon nanowire. The radius of curvature of the U-shaped nanowire (diameter = 80 nm) assembled on a copper TEM grid is 1.5 μm before cutting one arm with a FIB. After cutting the upper arm at the position indicated by the green arrow, the nanowire springs back to an almost straight configuration, suggesting that much of the strain introduced during U-shaped assembly of the nanowires is elastic.

Supplementary References

1. Yao, J.; Yan, H.; Lieber, C. M. *Nat. Nanotechnol*. **2013**, *8*, 329–335.
2. Yan, H.; Choe, H. S.; Nam, S. W.; Hu, Y.; Das, S.; Klemic, J. F.; Ellenbogen, J. C.; Lieber, C. M. *Nature* **2011**, *470*, 240–244.
3. Fan, Z.; Ho, J. C.; Jacobson, Z. A.; Yerushalmi, R.; Alley, R. L.; Razavi, H.; Javey, A. *Nano Lett.* **2008**, *8*, 20–25.
4. Stan, G.; Krylyuk, S.; Davydov, A. V.; Cook, R. F. *J. Mater. Res.* **2012**, *27*, 562–570.
5. Yao, J.; Yan, H.; Das, S.; Klemic, J. F.; Ellenbogen, J. C.; Lieber, C. M. *Proc. Natl. Acad. Sci. U. S. A.* **2014**, *111*, 2431–2435.
6. Qing, Q. Jiang, Z.; Xu, L.; Gao, R.; Mai, L.; Lieber, C. M. *Nat. Nanotechnol*. **2014**, *9*, 142–147.
7. Xu, L.; Jiang, Z.; Qing, Q.; Mai, L.; Zhang, Q.; Lieber, C. M. *Nano Lett.* **2013**, *13*, 746–751.
8. Xu, L.; Jiang, Z.; Mai, L.; Qing, Q. *Nano Lett.* **2014**, *14*, 3602–3607.